Monthly Notices
of the
ROYAL ASTRONOMICAL SOCIETY

MNRAS **493,** 70–77 (2020)
Advance Access publication 2020 January 24

doi:10.1093/mnras/staa208

Spinning and colour properties of the active asteroid (6478) Gault

Albino Carbognani ★ and Alberto Buzzoni ★

INAF – Osservatorio di Astrofisica e Scienza dello Spazio, Via Gobetti 93/3, I-40129 Bologna, Italy

Accepted 2020 January 21. Received 2020 January 21; in original form 2019 July 18

ABSTRACT

We report on accurate BVR_c observations of (6478) Gault, a 5–6 km diameter inner main-belt asteroid in the Phocaea family, notable for its sporadic, comet-like ejection of dust. This curious behaviour has been mainly interpreted as reconfigurations after YORP spin-up, although merging of a contact binary system cannot be fully excluded. We collected optical observations along the 2019 March–April period, at orbital phase angles between 12° and 21°, to search for direct evidence of asteroid quick spinning rotation. A prevailing period value of 3.34 ± 0.02 h is supported by our and other photometric observations. In the YORP spin-up hypothesis, this period points to a bulk density $\rho \approx 1$ g cm^{-3}. The mean colours are $B - V = +0.82_{\pm 0.3}$, $V - R_c = +0.28_{\pm 0.06}$, and $B - R_c = +1.11_{\pm 0.4}$, but we have observed a trend towards bluer colour during the April session, with about $\Delta(B - V) \sim 0.35 \pm 0.09$ mag. This colour change can be due to asteroid rotation and support the hypothesis that there is a bluer surface under the Gault's dust.

Key words: minor planets – asteroids: individual: (6478) Gault.

1 INTRODUCTION

Main belt asteroid (6478) Gault (hereafter 'Gault'), recently surged to very special attention (Smith & Denneau 2019) as an outstanding member of the active asteroids class, sporting typical morphological features of comets, such as a coma and tail (see Fig. 1). Pre-covery research in the NOAO image data base allowed to trace Gault's outbursts back to year 2013 (Chandler et al. 2019). As the outbursts appeared along the full heliocentric orbit, even about the aphelion distance of 2.75 au, this feature tends to exclude the sublimation of volatile material as a cause of the activity. Furthermore, spectroscopic observations showed a prevailing presence of dust, rather than gas, both in the coma and in the asteroid tails (Jewitt et al. 2019).

A re-iterate sequence of outbursts in the last year, namely on 2018 October 28 ± 5, December 31 ± 5, 2019 February 10 ± 7 (Jewitt et al. 2019), also including part of the present observations, may rule out as well the unlikely case of multiple impacts with smaller bodies as the triggering physical mechanism of Gault's activity. Rather, this may definitely restrain the focus to an intervening dynamical instability of the asteroid's structure, where a nearly spin-barrier rotation could strongly ease the on-going disintegration of a 'fluffy' body (Kleyna et al. 2019). Alternative to any rotation-driven process, however, also binary-system merging could be invoked as the main responsible of Gault's outbursts (Ye et al. 2019).

The presence of the spin-barrier in the 'realm of asteroids' can be explained by the cohesionless 'rubble-pile' structure model, assuming asteroids to consist in fact of collisional break-up fragments mainly bunching together under mutual gravitation, but in some case perturbed by centrifugal forces according to body's rotation speed (Pravec et al. 2002). Simple physical arguments lead to estimate, for the critical rotation period (P_S) of a spherical object of bulk density ρ (expressed in g cm^{-3})

$$P_S = \sqrt{\frac{3\pi}{G\rho}} \approx \frac{3.3\text{h}}{\sqrt{\rho}}. \quad (1)$$

Asteroid's bulk density is a crucial but difficult parameter to obtain, as we need to know both mass and volume of the body. In general, S-type asteroids are denser than C-type ones, the latter likely displaying a larger macroporosity. Reference figures indicate $\rho_S = 2.72_{\pm 0.54}$ g cm^{-3} for S-type and $\rho_C = 1.33_{\pm 0.58}$ g cm^{-3} for C-type objects (Carbognani 2017).

Things get slightly more entangled in case of a non-spherical geometry. If we deal in particular with the relevant case of a 'cigar-shaped' triaxial ellipsoid (spinning around the 'c' axis and with three axis constrain: $a \geq b = c$, according to Richardson, Elankumaran & Sanderson (2005), then the spin-barrier critical period (P_E) exceeds the spherical case of equation (1) as $P_E = \mathcal{F}\, P_S$, with the shape factor $\mathcal{F}(\epsilon)$ fully depending on body's (equatorial) eccentricity[1] in the form:

$$\mathcal{F} = \sqrt{\frac{2\epsilon^3}{3\left(\epsilon^2 - 1\right)\left(2\epsilon + \ln\frac{1-\epsilon}{1+\epsilon}\right)}}. \quad (2)$$

By combining equations (1) and (2), a straight P_E versus ρ relationship can be derived, as displayed in Fig. 2 for different values of eccentricity. According to previous bulk-density figures, one sees from the plot that centrifugal break-up may be reached by

★ E-mail: albino.carbognani@inaf.it (AC); alberto.buzzoni@inaf.it (AB)

[1] As usual, we define $\epsilon = [1 - (b/a)^2]^{1/2}$, in terms of minor-to-major axial ratio (b/a) of the body.

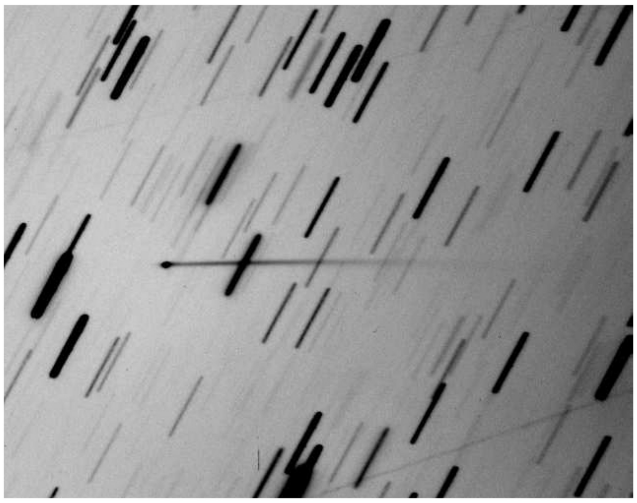

Figure 1. A 14 × 11 arcmin picture of (6478) Gault with its tail taken from OAVdA on 2019 March 23, about 20:20 UT ($\alpha = 10^{h}\ 04^{m}\ 25.2^{s}$, $\delta = -01^{\circ}\ 08'\ 06''.7$; J2000.0). North is up, east to the left. The main tail length is 5 arcmin 30 arcsec at position angle PA ≈ 272°. Its also visible a fainter 12 arcsec-extended antitail at PA ≈ 91°. The image is a stack of 38 frames, each with 180 s exposure time.

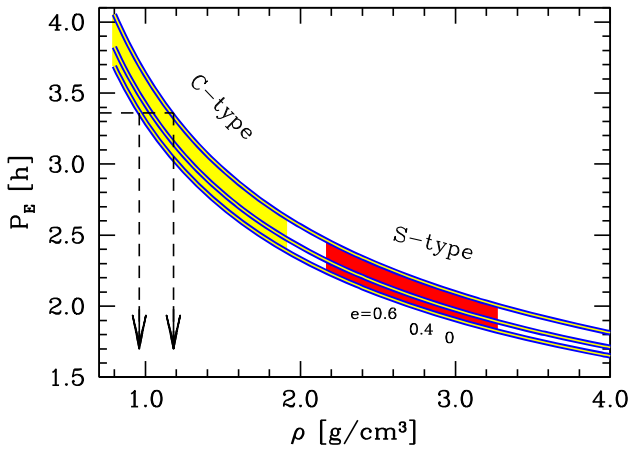

Figure 2. The expected P_E versus ρ relationship according to Richardson et al. (2005). Spin-barrier critical period P_E in case of a 'cigar-shaped' triaxial ellipsoid is obtained from the spherical case modulated by the shape factor $\mathcal{F}$ of equation (2), fully depending on the body's eccentricity. In addition to the spherical geometry ($e = 0$) two cases are displayed in the plot, respectively, with $e = 0.6$ and 0.4, with a slower critical period increasing with body's eccentricity, at fixed bulk density ρ, as labelled on the plot. The reference bulk-density figures for C- and S-type asteroids, according to Carbognani (2017) are reported as yellow and red bands, respectively. The prevailing estimate of Gault's rotation period of $P = 3.34$ h is marked in the plot, together with the implied range for asteroid's density (arrows) $\rho \sim 1$ g cm^{-3}. See text for a discussion.

C-type asteroids for a spin-barrier critical period $P_E \sim 2.5$–4.0 h, while a shorter period, always well less than 2.5 h, might be required for a denser S-type object.

No firm estimate of Gault's rotation period was available until cometary activity was first discovered on 2019 January 5 (Smith & Denneau 2019). Subsequent photometric follow-up to obtain an accurate light curve of the object did not lead to any conclusive result, likely due to the masking effect of dust in the coma (Jewitt et al. 2019; Kleyna et al. 2019; Man-To, Yoonyoung & Xing 2019; Sanchez et al. 2019; Ye et al. 2019). Based on a Lomb–Scargle and ANOVA light-curve analysis, Kleyna et al. (2019) recently proposed for Gault a rotation period about 2 h, which implied a density of about 2.7 g cm^{-3} as for a typical S-type asteroid. However, a slower period, about 3 h, more suitable for a C-type object, has later been claimed by Ferrin (2019). Until now, no phased light curve can be reported to explicitly support any of these values.

2 OBSERVATIONS AND DATA REDUCTION

Thanks to asteroid's closer distance, near opposition with Earth, and taking advantage of the declining trend of dust activity, we surveyed Gault along the 2019 March–April trajectory arc, with the purpose of determining the asteroid's rotation period from its optical light curve. A first observing batch was carried out with the OAVdA Ritchey–Chrétien 0.81-m *f*/4.75 telescope at Saint-Barthelemy (Aosta, Italy, MPC ID code B04) along the three nights of 2019 March 23, 26, and 27. The sky was with some sporadic veils the first night, while in the following two nights it was clear and transparent. The telescope was equipped with an FLI 1001E CCD array of 1024 × 1024 pixels with 24 μm pixel size used in 2 × 2 binning mode such as to provide a platescale of 2.54 arcsec px^{-1} across a 21.9 × 21.9 arcmin field of view. Gault's imaging was performed with *C* filter (i.e. 'white light'), in order to maximize target detection (estimated about $V \sim 17$). The frames were dark subtracted and then flat-fielded according to the standard procedure. The SNR for the three sessions was near 50, the mean uncertainty is, respectively, 0.020, 0.022, and 0.023 mag. Although fully successful ones, these observations caught the asteroid still in full activity, with a detectable coma and an extended dust tail visible over 5.5 arcmin away at $PA \sim 272^{\circ}$, as well evident from Fig. 1.

A further observing run was then attempted one month later, along the night of 2019 April 15, with the asteroid now definitely 'turned off' in its quiescent state (see Fig. 3). However, as Gault was becoming about one magnitude fainter with increasing its orbital phase angle, we had to rely on the larger 'G.B. Cassini' 152 cm *f*/4.6 Ritchey–Chrétien telescope of the Loiano Observatory (Bologna, Italy, MPC ID code 598) for these new observations. The BFOSC camera was attached the telescope, equipped with a Princeton Instruments EEV 1340 × 1300 pixel back-illuminated CCD with 20 μm pixel size. Platescale was 0.58 arcsec px^{-1} leading to a field of view of 13.0 × 12.6 arcmin. Broad-band Johnson/Cousins *B*, *V*, R_c filters were used to measure asteroid's colours. The telescope was tracked at non-sidereal rates to follow Gault's motion and increase S/N of detection.

The Loiano observations were carried out under clear but partly scattered sky, with seeing about 2.2 arcsec [full width at half-maximum (FWHM)] and a bright full Moon about 12° apart from the target. Nevertheless, a good sequence of R_c images each with 240 s integration (mean uncertainty about 0.09 mag), was obtained spanning about 4 h in total, interleaved by three *B*, *V* series to sample asteroid's colours. The Landolt (1992) PG1047+003 calibration field was taken at similar airmass of Gault images in the three *B*, *V*, R_c bands, providing to avoid cloud interference. Image processing included bias subtraction and flat-fielding procedure, as usual. Due to scattered clouds, however, special care has been devoted for photometric reduction of the entire data set, as discussed in more detail in the next sections. Along the total of four OAVdA and Loiano observing runs, we collected about 12 h of observation on the target, as summarized in Table 1.

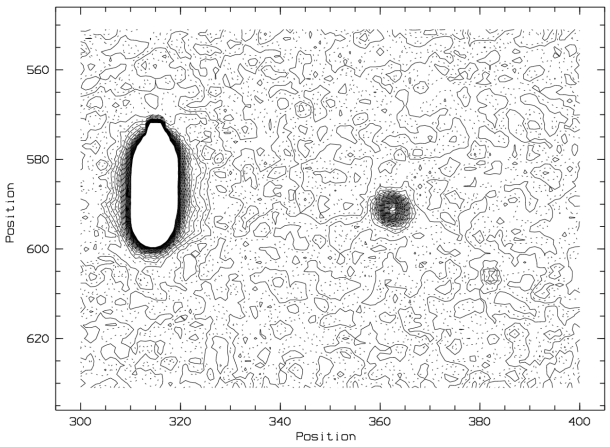

Figure 3. R_c-band isophotal contour plot of a Gault's illustrative image from the Loiano data set, along the night of 2019 April 15. Esposure time is 240 s with telescope tracked at non-sidereal rates to follow Gault's motion. The displayed field of view is about 60 × 45 arcsec across, with North up and East to the left. Coordinate axes are labelled in pixel scale (1 px = 0.58 arcsec). Gault is the 'rounded' object about $(x, y) = (362, 591)$ coordinates. The vertically elongated object to the left of the image is a saturated star distorted by on-target tracking. Seeing on the image is about 2.2 arcsec FWHM. A bright full Moon, only 12° apart was strongly affecting the sky background, here estimated in $\mu_R \sim 16.8$ mag arcsec^{-2}. From the image, we can however rule out at an S/N ≥ 3 confidence level any activity signature around the asteroid, brighter than 21.9 mag arcsec^{-2}.

Table 1. Summary of the 2019 OAVdA (B04) and Loiano (598) observing sessions.

Date	No. of frames	Band	Exposure (s)	Timespan (h)	MPC ID
March 23	47	C	180	2.0	B04
March 26	61	C	180	3.0	B04
March 27	65	C	180	3.0	B04
April 15	49	R_c	240	4.0	598
	3	V	300		598
	3	B	480		598

2.1 On-frame photometry

MPO Canopus package (Warner 2009) was used for differential aperture photometry of our data. We especially relied on the Comp Star Selector (CSS) and Derivedmags software feature to pick up a reference grid of (whenever possible) solar-type standards, from the CMC15 star catalogue (Muiños & Montojo 2014), and therefrom lead to an accurate calibration (to within a few hundredths of magnitude internal uncertainty) of Gault' magnitude directly on the observed field. This is very useful because it allows the different photometric sessions to be linked together. Gault's aperture photometry has been carried out through an ∼3 FWHM circular aperture, throughout, to account for seeing effects. Only the best frames, with the target clearly unaffected by star crowding, were retained. According to the CMC15/UCAC4/APASS photometric characterization (Carbognani 2016), we can confidently match the Johnson–Cousins R_c system with our observations with the equation:

$$R_c = r' - 0.112 - 0.128\,(B - V) \quad \text{mag}. \tag{3}$$

In equation (3) r' is the apparent red mag of the star in the Sloan system adopted by CMC15/UCAC4/APASS catalogues, while B and V are the mag in the Johnson system. The RMS, when using equation (3), is about 0.05 mag. For a solar-type star, as our comparisons, $B - V \simeq 0.656 \pm 0.005$, so:

$$R_c \simeq r' - 0.2 \tag{4}$$

This and the previous correction was applied throughout in the reported R_c magnitudes of this paper. A subset of three-to-five comparison stars across the full frame sequence for each observing run were measured in order to assess sky transparency conditions along the night. In particular, for the Loiano observations, this procedure allowed us to track in some detail the temporal behaviour of thin cloud absorption affecting Gault's imaging and recover colours to fiducially cloud-free conditions. This correction is of paramount importance in order to derive the asteroid's colours variation.

Table 2. UCAC4 stars BVR_c colours along the observing night of 2019 April 15. The last two columns provide, respectively, the average colour value on three Batch and the catalogue value.

473-044752	Batch #1	Batch #2	Batch #3	Average	Cat.
$B - V$	$0.33_{\pm 0.03}$	$0.34_{\pm 0.03}$	$0.52_{\pm 0.03}$	$0.40_{\pm 0.06}$	0.43
$V - R_c$	$0.23_{\pm 0.02}$	$0.27_{\pm 0.02}$	$0.27_{\pm 0.02}$	$0.26_{\pm 0.01}$	0.25
$B - R_c$	$0.56_{\pm 0.02}$	$0.61_{\pm 0.02}$	$0.79_{\pm 0.02}$	$0.66_{\pm 0.07}$	0.68
473-044753					
$B - V$	$0.75_{\pm 0.04}$	$0.76_{\pm 0.04}$	$0.96_{\pm 0.04}$	$0.82_{\pm 0.07}$	0.90
$V - R_c$	$0.39_{\pm 0.02}$	$0.46_{\pm 0.02}$	$0.44_{\pm 0.02}$	$0.43_{\pm 0.02}$	0.41
$B - R_c$	$1.14_{\pm 0.03}$	$1.22_{\pm 0.03}$	$1.40_{\pm 0.03}$	$1.25_{\pm 0.08}$	1.32
473-044754					
$B - V$	$1.42_{\pm 0.06}$	$1.37_{\pm 0.06}$	$1.49_{\pm 0.06}$	$1.43_{\pm 0.04}$	1.49
$V - R_c$	$0.90_{\pm 0.04}$	$0.96_{\pm 0.04}$	$0.95_{\pm 0.04}$	$0.94_{\pm 0.02}$	0.93
$B - R_c$	$2.32_{\pm 0.05}$	$2.33_{\pm 0.05}$	$2.45_{\pm 0.05}$	$2.37_{\pm 0.04}$	2.42

3 GAULT'S COLOURS

Three series of deeper B, V images (referred to hereafter as Batch #1, 2, and 3, with exposure time of 8 min in B and 5 min in V) have been accompanying the R_c-band sequence along the Loiano session of 2019 April 15. As marked in the lower panel of Fig. 5, the B, V luminosity was sampled around 20:03-20:17 UT (Batch #1), 21:06-21:20 UT (Batch #2), and 22:10-22:24 UT (Batch #3), in order to assess Gault's apparent colours at different light-curve phase. The photometric reduction has been carried out according to the usual standard calibration procedure (Harris, Fitzgerald & Reed 1981; Landolt 1992). In addition, special care has been devoted to take the Landolt field at similar airmass than Gault's frames in order to minimize differential corrections.

If we look at the photometric trend of the comparison stars present in Gault's field of view we see that cloud absorption did not affect Batch #1, while a thinner coverage was in place, on the contrary, at Batch #2 and Batch #3. To estimate the effect of cloud absorption on colours we chose three stars, from the UCAC4 (Zacharias et al. 2013) stars catalogue,[2] placed near Gault and computed the colours with the same photometric parameters used for Gault. The results are shown in Table 2. From this we can see how the average colours value and the one from the UCAC4 catalogue are

[2]In the UCAC4 catalogue the B and V mag are in the Johnson system, while the red mag are in the Sloan r' system. To transform from r' to R_c, we use equation (3).

Table 3. The mean colours correction terms for Batch #1, Batch #2, and Batch #3 derived from colours of Table 2.

	Batch #1	Batch #2	Batch #3
$B-V$	0	$+0.01_{\pm 0.03}$	$-0.16_{\pm 0.07}$
$V-R_c$	0	$-0.06_{\pm 0.01}$	$-0.05_{\pm 0.006}$
$B-R_c$	0	$-0.05_{\pm 0.03}$	$-0.21_{\pm 0.07}$

Table 4. Gault's BVR_c colours along the observing night of 2019 April 15, and comparison with Man-To et al. (2019). The trend towards bluer colour from Batch #1 to Batch #3 is evident (see also Fig. 4).

	Batch #1[a]	Batch #2[a]	Batch #3[a]	Average	MT19[b]
$B-V$	$0.84_{\pm 0.04}$	$1.15_{\pm 0.06}$	$0.49_{\pm 0.08}$	$0.82_{\pm 0.3}$	$0.79_{\pm 0.06}$
$V-R_c$	$0.34_{\pm 0.02}$	$0.29_{\pm 0.03}$	$0.22_{\pm 0.02}$	$0.28_{\pm 0.06}$	$0.31_{\pm 0.02}$
$B-R_c$	$1.19_{\pm 0.03}$	$1.44_{\pm 0.05}$	$0.71_{\pm 0.08}$	$1.11_{\pm 0.4}$	$1.10_{\pm 0.06}$

[a] After cloud veils correction, as discussed in the text.
[b] As from Man-To et al. (2019).

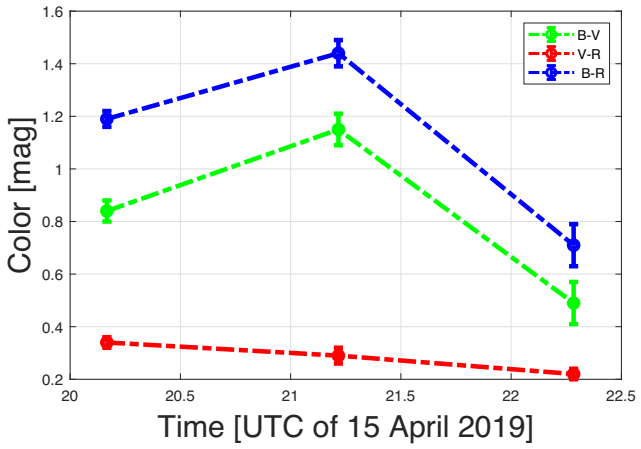

Figure 4. Gault's colours variations over time.

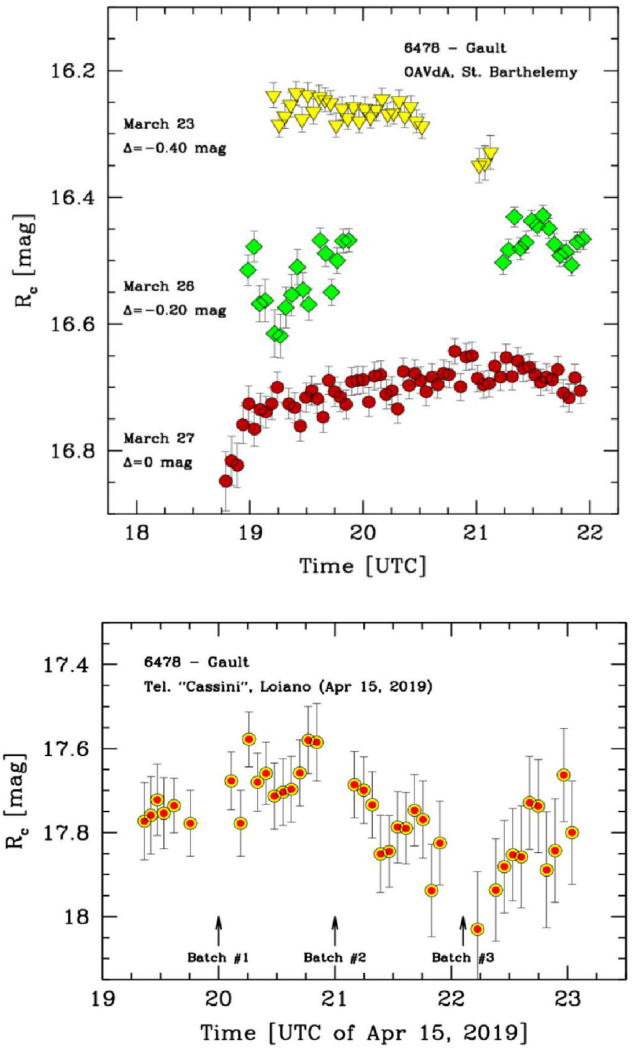

Figure 5. Gault's observing sessions of 2019 March 23–27 from OAVdA (the mean uncertainty for the three sessions are, respectively, 0.020, 0.022, and 0.023 mag) and 2019 April 15 from Loiano (mean uncertainty 0.09 mag), are summarized in the upper and lower panels, respectively. The R_c magnitude scale is reproduced, throughout, from the local CMC-15 calibration, according to equation (4). Along the OAVdA observations, the asteroid was about its Earth opposition, at orbital phase angle $\phi \sim 12.9°$, a figure that increased to $\phi \sim 21.4°$ for the Loiano data. The B, V magnitude sampling from Batch #1–3 observations is marked on the plot. Note a substantial difference in light-curve amplitude and shape between the two observing sessions. See text for a discussion.

compatible within a few hundredths of magnitude. Thus, despite the presence of veils and the full Moon, the observed colours are reliable. If we look at the individual Batches, we can see how the stars colours tend to become redder, going from Batch #1 to Batch #3 as expected, which appears to be the most conditioned by cloud veils. Taking as reference the Batch #1, we can compute a set of mean correction terms defined as (colours Batch #1)-(colours Batch #2) or (colours Batch #1)-(colours Batch #3). We can use these additive terms to 'delete' the veils effect on Gault's colours (see Table 3).

The apparent Gault colours along the three observing windows are displayed in Table 4, together with their average values. As far as the latter ones are considered, our colours are fully consistent with Man-To et al. (2019), after correcting the latter ones to the Johnson–Cousins system, according to Bessel (1979). One has to report, however, the evident trend towards 'bluer colour' along the Table 4 observations (see Fig. 4 for a plot), with the asteroid becoming increasingly bluer of about $\Delta(B-V) \sim 0.35 \pm 0.09$ mag, near the luminosity minimum (see Fig. 5). This trend was not present in the UCAC4 stars of Table 2, where, on the contrary, there is a little redshift due to veils, as expected. We consider this trend towards bluer colour a real effect. Probably there is a bluer region on the Gault surface that we had observed during the session, thanks to asteroid rotation. Indeed, the temporal difference between Batch #1 and Batch #3 is about 2 h, more than half of the best rotation period we estimated for Gault (see Section 4.1). These colours variation towards blue is consistent with what was found by Marsset et al. (2019), that in NIR spectroscopic observations of 2019 March 31 found Gault bluer than similar observations of 2019 April 8. In this last observation the Gault spectrum appears an S-type asteroid, compatible with Phocaea's spectrum. To our knowledge, no one had observed such a marked change in Gault's colour during the same session. It is assumed as a rule that the surface of asteroids is uniform so finding these changes, as for NEA (297274) 1996 SK (Lin et al. 2014), is very interesting.

4 DERIVED LIGHT CURVE

A general summary of the OAVdA and Loiano observations is summarized in the two panels of Fig. 5. As far as the OAVdA data set is concerned, a first outstanding feature of Gault's observed light curve along all the three nights of 2019 March 23, 26, and 27 is a quite regular trend with the object almost steady at a 'flat' maximum interspersed with 'spiky' minima, where magnitude gets some 0.1–0.15 mag fainter.

This feature, strongly reminiscent of the photometric behaviour of eclipsing binary stars, closely recalls a similar trend seen weeks before by the Indian HCT and ESA OGS telescopes, as reported by Kleyna et al. (2019, see their fig. 3). A change of status occurs, however, in the April observations from Loiano (lower panel of the figure) where, on the contrary, the asteroid variation shows a smoother 'sinusoidal' light curve and much larger amplitude (i.e. $A_{Rc} \sim 0.5$ mag).

Such a strong change in the light-curve amplitude and shape prevented us from put all observing sessions together in a coherent period analysis. However, one may argue that this photometric behaviour is typical of an elongated body as the orbital phase angle (ϕ) increases. In fact, the observations from the HCT and OGS telescopes, and from OAVdA as well were taken close to asteroid's opposition, at the mean orbital phase angle $\phi \sim 10^\circ \pm 3^\circ$ and 12.9°, respectively, while from Loiano we observed at a phase angle $\phi = 21.4^\circ$.

A distinctive relationship is recognized for asteroids of different taxonomic type between amplitude and orbital phase angle (Zappalá et al. 1990) in the form:

$$A(\phi) = A(0)\,(1 + m\phi). \tag{5}$$

In the equation, $A(0)$ is the light-curve amplitude (in mag) at the opposition (namely at $\phi = 0^o$). If we express ϕ in degrees, then the scaling coefficient m depends on the taxonomic type and can be empirically calibrated (Zappalá et al. 1990) as $m = 0.030$, 0.015, and 0.013, respectively for S-, C-, and M-type asteroids.

If we enter l.h. term of equation (5) with the amplitude observed from Loiano, that is $A(21.4^\circ) \approx 0.5$ mag, which is our best value as observed when Gault's activity was decreasing, then an opposition value of $A(0) = 0.35_{\pm 0.05}$ mag is inferred, accounting for the full range of m along the taxonomic class. If we assume the magnitude variation to be fully induced by a change of reflective surface in a 'cigar-shaped' ellipsoid (with fixed albedo), then the (b/a) ratio can be constrained as $(b/a) \approx 10^{-0.4\,A(0)} = 0.73_{\pm 0.03}$. According to footnote 1 definition, this leads to a plausible range for body's (sagittal) eccentricity of $\epsilon \approx 0.68_{\pm 0.03}$. This estimate implies that the light-curve amplitude is due entirely to the asteroid shape. If there are albedo patches on surface, as discussed above, the elongation will be smaller.

4.1 Rotation and spin-barrier critical period

Given our sparse data set, a more pondered statistical approach was pursued to constrain the possible periodicity in Gault's light curve. The OAVdA data are better suited for this exercise because they span a larger timeline, between March 23 and 27. On the contrary, the Loiano observations restrain to a 4 h interval only, although they more firmly appear to constrain the allowed range of possible period values, yet hardly shorter than 3 h (see Fig. 5). To further extend the temporal coverage of the OAVdA's photometry, data taken from Sanchez et al. (2019) on March 26 and 30, 2019 were also used (see Fig. 6) in our analysis. We did a Lomb–Scargle analysis, between

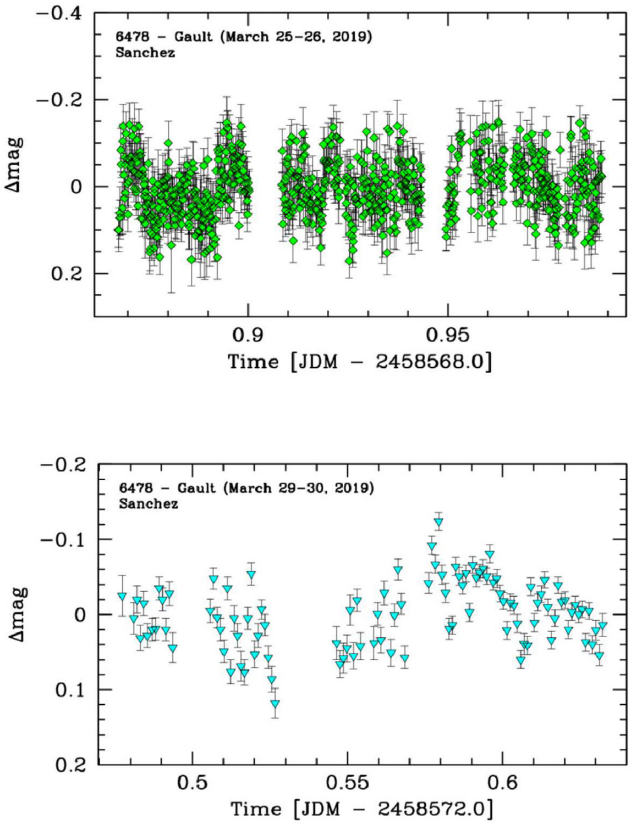

Figure 6. Gault's observing sessions of 2019 March 26 and 30 from Sanchez et al. (2019) are summarized in the upper and lower panels, respectively.

0.5 and 10 h, of the Gault light curve using all the OAVdA and Sanchez sessions. If all sessions are used, the dominant period is 1.3 h completely given by the March 26 Sanchez session. This peak is a fake, due to two interruptions in the observations at a distance of 0.05 d, or about 1.2 h which gives a false periodicity in a substantially flat light curve. Another problem with the March 26 Sanchez session is that the average error on the mag is 0.05, while for the OAVdA and Sanchez sessions on March 30 it goes from 0.015 to 0.023. So Sanchez's March 26th session is twice as noisy as the others and it makes sense to remove it from the analysis. Removing this session the best period is 3.34 ± 0.02 h (see Fig. 7). In the periodogram remains a widened peak between 7 and 8 h, which could correspond to the period of a hypothetical binary system, see Section 4.2 for a more detailed discussion. This value also confirms the Ferrin (2019) preliminary estimate from his own photometry, and the period is also compatible with the Loiano observations, as evident from the plot of Fig. 5. Indeed, a Lomb–Scargle analysis of the Loiano data set also show a peak around a period of about 3.4 h.

Our results were also corroborated by independently cross-checking the OAVdA and Sanchez data with the FALC Fourier analysis algorithm by Harris et al. (1989), implemented in the MPO CANOPUS package. The resulting MPO Canopus phased light curves from OAVdA and Sanchez are shown in Fig. 8. The best period is 3.36 h very close to the 3.34 h period that we had found using Lomb–Scargle. One major concern deals with the lack of any evident 'secondary' minimum, about mid-way from two 'primary' minima (i.e. 'double-peaked' light curve), as usual for an

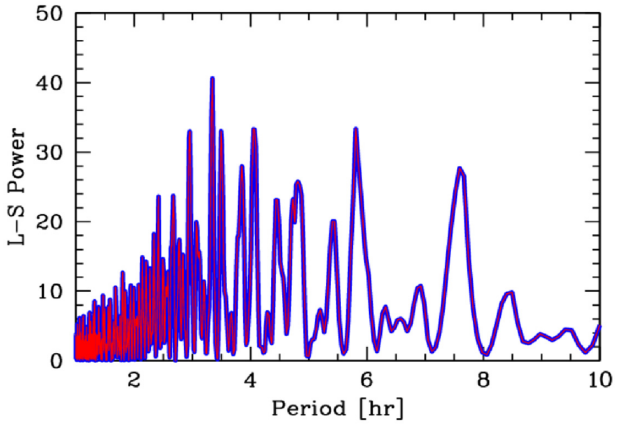

Figure 7. The Lomb–Scargle periodogram of spectral power versus period (between 0.5 and 10 h) for OAVdA's sessions and Sanchez 30 March. The best period is 3.34 ± 0.02 h.

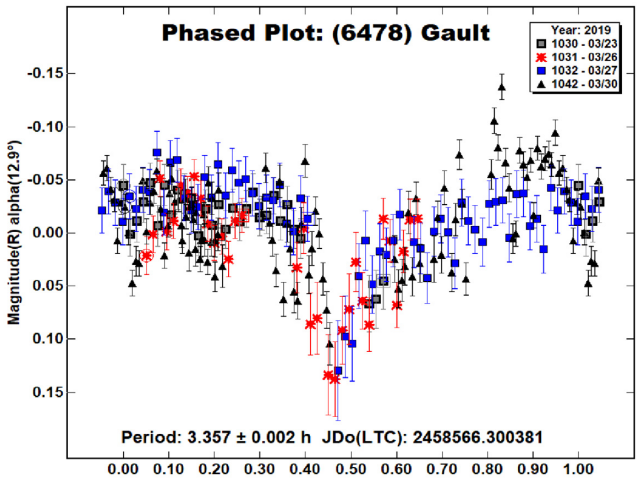

Figure 8. The phased light curves of the March 23, 26, 27 OAVdA, and March 30 Sanchez according to the Falc algorithm implemented in MPO Canopus. In this case, the best period is 3.36 h, very near to the 3.34 ± 0.02 h best period of Fig. 7, found with the Lomb–Scargle periodogram.

asteroids. Probably Gault's reflectance have been heavily affected by dust activity which may have partially erased the light-curve characteristics.

In a disrupting 'rubble-pile' structure model, a glance to Fig. 2 clearly points to an asteroid bulk density $\rho \lesssim 1.2$ g cm^{-3}, a value compatible with a internally fragmented S-type asteroid, i.e. with large macroporosity. As a main conclusion, our analysis definitely rules out the spin-barrier classical value of about 2 h, as claimed by Kleyna et al. (2019).

4.2 A merging binary system?

Patching absorption by Gault's surrounding dust layers could naturally give reason of the the lack of any 'secondary' minimum in the phased light curves of Fig. 8[3] and the so erratic luminosity trend

[3]Actually, in a dust-free 'cigar-shaped' ellipsoid of fixed albedo, spinning around the principal momentum axis, one *must* expect 'secondary' minimum to be of equal amplitude than the 'primary' one, both being generated by the opposite end-to-end extrema of the spinning 'cigar'.

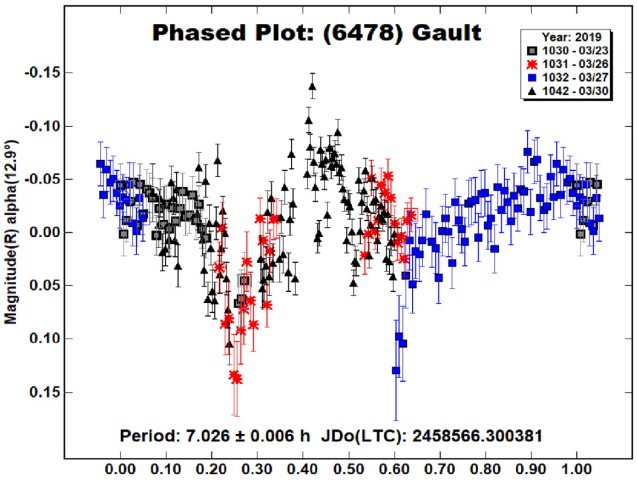

Figure 9. The phased light curves of the March 23, 26, 27 OAVdA, and March 30 Sanchez according to the Falc algorithm implemented in MPO Canopus but plotted with the ∼2 × period values. This light curve, with a best period of about 7 h, is compatible with a contact binary system with equal components (Descamps 2008).

discussed in the Kleyna et al. (2019) paper, as well. Alternatively, we can match the expected 'double-peaked' photometric trend by moving on the ∼2 × period pattern. The resulting phased light curve of the OAVdA and Sanchez data given by MPO Canopus, is shown in Fig. 9. Such new physical scenario, with a best period of about 7 h, could explain Gault's activity in terms of a near-contact binary that merge itself in a contact binary through the loss of angular momentum due to BYORP effect (Ye et al. 2019). Indeed a careful analysis of Fig. 9 may recall a contact binary system of two elongated bodies of similar size whose orbital plane is tilted enough with respect to our point of view such as to avoid full occultation between the two components (see e.g. Descamps 2008, for illustrative examples). Note that the second minimum in Fig. 9 does not fall exactly at the 0.75 phase as expected for a contact binary system, probably the light curve is 'dirty' as a result of Gault's activity (with OAVdA's session only, the second minimum fall in 0.75 phase). In this case, if we assume the same bulk density (ρ_G) and size (R_G) for the two Gault's components, orbiting at a distance $n\ R_G$ apart,[4] then the Kepler third law provides:

$$\frac{4\,\pi^2}{P^2} = \rho_G\, G \frac{(8/3)\,\pi R_G^3}{(n\ R_G)^3}, \tag{6}$$

or

$$P = \sqrt{\frac{3\pi\, n^3}{2\,G}\,\frac{1}{\rho}} \sim \frac{2.33\, n^{3/2}}{\sqrt{\rho}} \quad \text{(hr)} \tag{7}$$

Fig. 10 summarizes our results for the full range of possible configurations. In case of a preferred fiducial period of $P \approx 7$ h or larger, a contact double asteroid could be admitted with an implied bulk density $\rho \lesssim 1.0$ g cm^{-3}, as marked in the figure. A much larger value for ρ would however allowed in case of a close but semidetached system.

[4]In our notation, we have a contact binary if $n = 2$, that is if the two asteroid components are separated by twice their reference radius R_G.

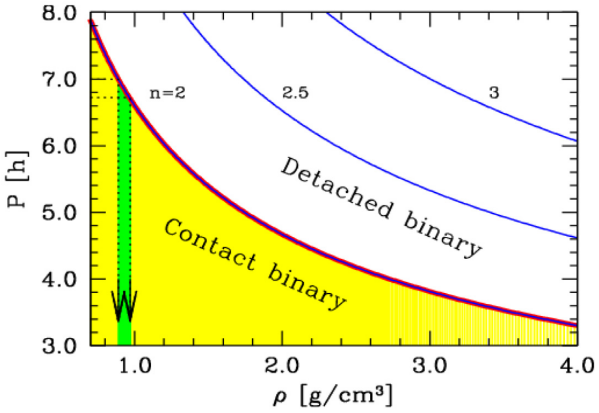

Figure 10. The expected P versus ρ relationship for a close binary system with the asteroid consisting of two components of similar size and mass, according to equation (7). The component distance is parametrized in terms of multiple 'n' of the body's reference radius, R_G, as in equation (6). Accordingly, a contact system is obtained for $n = 2$, while for $n = 3$ the two asteroid components are orbiting one R_G apart. The nominal periodicity of case $P \approx 7$ h is singled out in the plot, with an implied density for Gault of $\rho \lesssim 1.0$ g cm^{-3}, in case of a contact binary system. The 6.7-h double periodicity, that occurred in MPO Canopus without using the March 30 Sanchez session, is also indicated. This gives an idea of the 'weight' that even a single session can have in these critical measures.

5 SUMMARY AND CONCLUSIONS

In this paper, we comprehensively reviewed the observations made in early 2019 on the new active asteroid (6478) Gault. The most likely cause is that the asteroid activity was due to reconfigurations after YORP spin-up. However, also binary-system merging could be invoked as the main responsible of Gault's outbursts. For this reason an accurate estimate of the inherent photometric periodicity could actually discriminate between the different scenarios. Until very recently, in their 2019 observations, Kleyna et al. (2019) proposed a spinning value about 2 h, which implied a density of some 2.7 g cm^{-3}, as for a typical S-type asteroid (see Fig. 2). This result was consistent with Gault's asteroid family: Phocaea. Two NIR spectra taken by Marsset et al. (2019) show deep absorption band near 1 and 2 μm consistent with an S-type asteroid, this support the link between Phocaea collisional family and Gault. To better clarify the situation about the rotation period, we added fresh photometric observations from OAVdA, in the second half of 2019 March (see Fig. 5). To extend the temporal coverage of the OAVdA's photometry, data taken from Sanchez et al. (2019) on 2019 March 26 and 30, were also used (see Fig. 6). Finally we did a Lomb–Scargle analysis, between 0.5 and 10 h, of the Gault light curves using OAVdA and Sanchez sessions. From the periodogram (see Fig. 7), a best period is identified, namely $3.34_{\pm 0.02}$ h, with no evident sign of any ∼2 h periodicity. The 3.34 h period also confirms the Ferrin (2019) preliminary estimate and it may be taken as the most probable, although the other near values cannot be firmly excluded at the current state of observations. If this is the real context, then by invoking the spin-barrier limit, Fig. 2 shows that Gault's bulk density should not exceed $\rho \sim 1.2$ g cm^{-3}, compatible with a fragmented S-type asteroid. By forcing twice a photometric period in order to fit with a 'double-peaked' light curve (Fig. 9), we challenged the possibility for Gault to be a merging contact (or semidetached) binary system consisting in fact of similar twin bodies. A realistic solution in this case points to a best period of about 7 h, leading to quite a 'fluffy' bulk density $\rho \lesssim 1.0$ g cm^{-3}, in force of equation (7).

The mid-April light curve from Loiano, sampling Gault's more quiescent status compared to March (see Fig. 3 and compare with Fig. 1), shows a greater amplitude and a more sinusoidal shape compared to the OAVdA observations. Also this data set show a peak around a period of about 3.4 h. In case of constant albedo, this may be suggestive of an elongated (roughly cigar-like) shape for the body, with an implied (sagittal) eccentricity $\epsilon \approx 0.68_{\pm 0.03}$.

Gault colours were also assessed along the Loiano observing run, leading to the average figures summarized in Table 4, namely $(B - V) = 0.82_{\pm 0.3}$, $(V - R_c) = 0.28_{\pm 0.06}$ and $(B - R_c) = 1.11_{\pm 0.4}$, in quite a good agreement with Man-To et al. (2019) but with a remarkable trend towards bluer colour, with the asteroid becoming much bluer near the minimum light-curve luminosity (see Fig. 5). The change in $(B - V)$ colour was about $\Delta(B - V) \sim 0.35 \pm 0.09$ mag. This strange behaviour is supported by the aforementioned spectroscopic observations made on March 31 and April 8 by Marsset et al. (2019). The first spectrum was bluer than the second one and this indicates a macroscopic difference of albedo in different Gault's areas. It is possible that this difference is due to an active area that has exposed new fresh material not been reddened by solar radiation. Further photometric and spectroscopic observations are needed to fully characterize this very interesting minor body.

ACKNOWLEDGEMENTS

The authors wish to thank Sanchez J. A. for granting the use of Gault photometric data and the Astronomical Observatory of the Autonomous Region of the Aosta Valley (OAVdA), managed by the Fondazione Clément Fillietroz-ONLUS, for granting the use of the Main Telescope. Many thanks to the referee for the useful suggestions that have greatly improved the quality of the manuscript.

REFERENCES

Bessell M. S., 1979, PASP, 91, 589
Carbognani A., 2016, Minor Planet Bull., 43, 290
Carbognani A., 2017, Planet. Space Sci., 147, 1
Chandler C. O., Kueny J., Gustafsson A., Trujillo C. A., Robinson T. D., Trilling D. E., 2019, ApJ, 877, L12
Descamps P., 2008, Planet. Space Sci., 56, 1839
Ferrin I., 2019, Astron. Telegram, 12663
Harris A. W. et al., 1989, Icarus, 77, 171
Harris W. E., Fitzgerald M. P., Reed B. C., 1981, PASP, 93, 507
Jewitt D., Kim Y., Luu J., Rajagopa J., Kotulla R., Ridgway S., Liu W., 2019, ApJ, 876, L19
Kleyna J. T. et al., 2019, ApJ, 874, L20
Landolt A. U., 1992, AJ, 104, 340
Lin C. H. et al., 2014, Res. Astron. Astrophys., 14, 311
Man-To H., Yoonyoung K., Xing G., 2019, MNRAS, 488, L143
Marsset M. et al., 2019, ApJL, 882, L2
Muiños J. L., Montojo J., 2014, The Carlsberg Meridian Catalog, Niels Bohr Institute U. o. C., Inst. of Astronomy C., UK
Pravec P., Kušnirák P., Šarounová L., Harris A. W., Binzel R. P., Rivkin A. S., 2002, ESA SP-500, Large coherent asteroid 2001 OE_{84}. ESA, Noordwijk, p. 743

Richardson D. C., Elankumaran P., Sanderson R. E., 2005, Icarus, 173, 349
Sanchez J. A., Reddy V., Thirouin A., Wright E. L., Linder T. R., Kareta T., Sharkey B., 2019, ApJ, 881, L6
Smith K. W., Denneau L., 2019, CBAT, 4594, 1
Warner B. D., 2009, MPO Software, Canopus. Bdw Publishing, Eaton, Colorado (USA)
Ye Q. et al., 2019, ApJ, 874, L16
Zacharias N., Finch C. T., Girard T. M., Henden A., Bartlett J. L., Monet D. G., Zacharias M. I., 2013, AJ, 145, 44
Zappalá V., Cellino A., Barucci A. M., Fulchignoni M., Lupishko D. F., 1990, A&A, 231, 548

This paper has been typeset from a TEX/LATEX file prepared by the author.